eLIFE elifesciences.org

RESEARCH ARTICLE

Figures and figure supplements

Morphogenetic degeneracies in the actomyosin cortex

Sundar Ram Naganathan *et al*

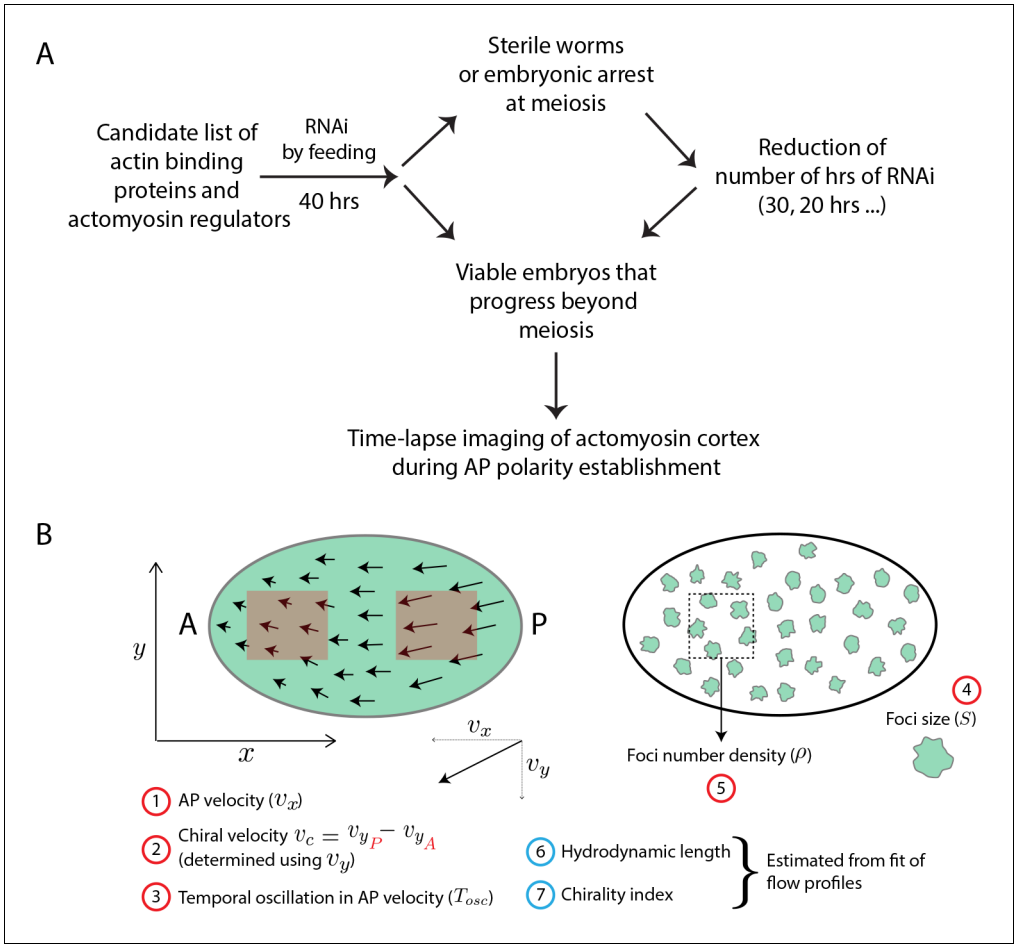

Figure 1. Screen strategy. (**A**) Flow chart describes strategy undertaken to perform candidate RNAi screen of actin binding proteins and actomyosin regulators. Time-lapse images were then used to determine flow properties of the cortex. (**B**) Schematic of a 1-cell embryo indicating the quantities measured (numbers in red circle) and estimated (numbers in blue circle). Left - 1-cell embryo, where arrows indicate flow velocities and arrow lengths signify magnitude. A, anterior and P, posterior of the embryo; x-axis is along the long-axis of the embryo and the y-axis orthogonal to it. Red boxes within embryo indicate analysis regions in the posterior and anterior. Right - 1-cell embryo with myosin foci (green blobs).

DOI: https://doi.org/10.7554/eLife.37677.002

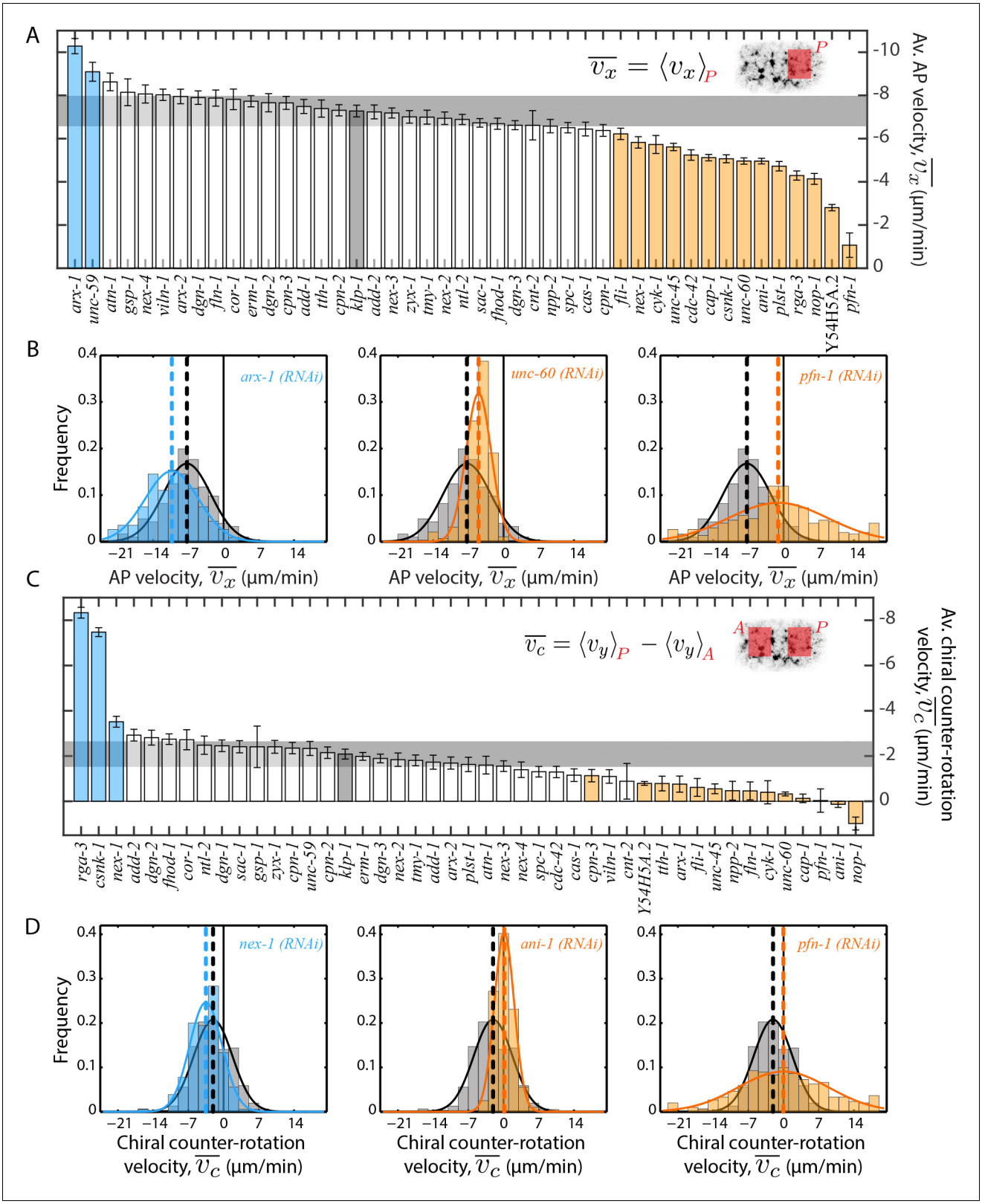

Figure 2. Quantification of cortical flow velocities. (**A**), (**C**) Comparison of mean AP velocity $\overline{v_x}$ and mean chiral counter-rotation velocity $\overline{v_c}$ respectively. Shaded areas in the inset represent regions over which the spatial average was performed in each time frame. Error bars, SEM; gray bar, negative control, *klp-1 (RNAi)* condition; gray horizontal bar, error of the mean with 99% confidence for *klp-1 (RNAi)*; cyan, beige bars, significantly different

Figure 2 continued on next page

Figure 2 continued

knockdowns with 99% confidence (Wilcoxon rank sum test). (**B**), (**D**) Representative histograms of instantaneous $\overline{v_x}$ and $\overline{v_c}$ respectively. Gray histograms, *klp-1 (RNAi)* condition; dashed lines, mean $\overline{v_x}$ and $\overline{v_c}$ respectively. See ***Figure 2—figure supplement 1*** and ***Figure 2—figure supplement 2*** for histograms of significantly different ABPs and ***Figure 2—figure supplement 3*** for a comparison of mean magnitude velocities. See Supplementary file for number of independent embryo samples in each RNAi condition.

DOI: https://doi.org/10.7554/eLife.37677.003

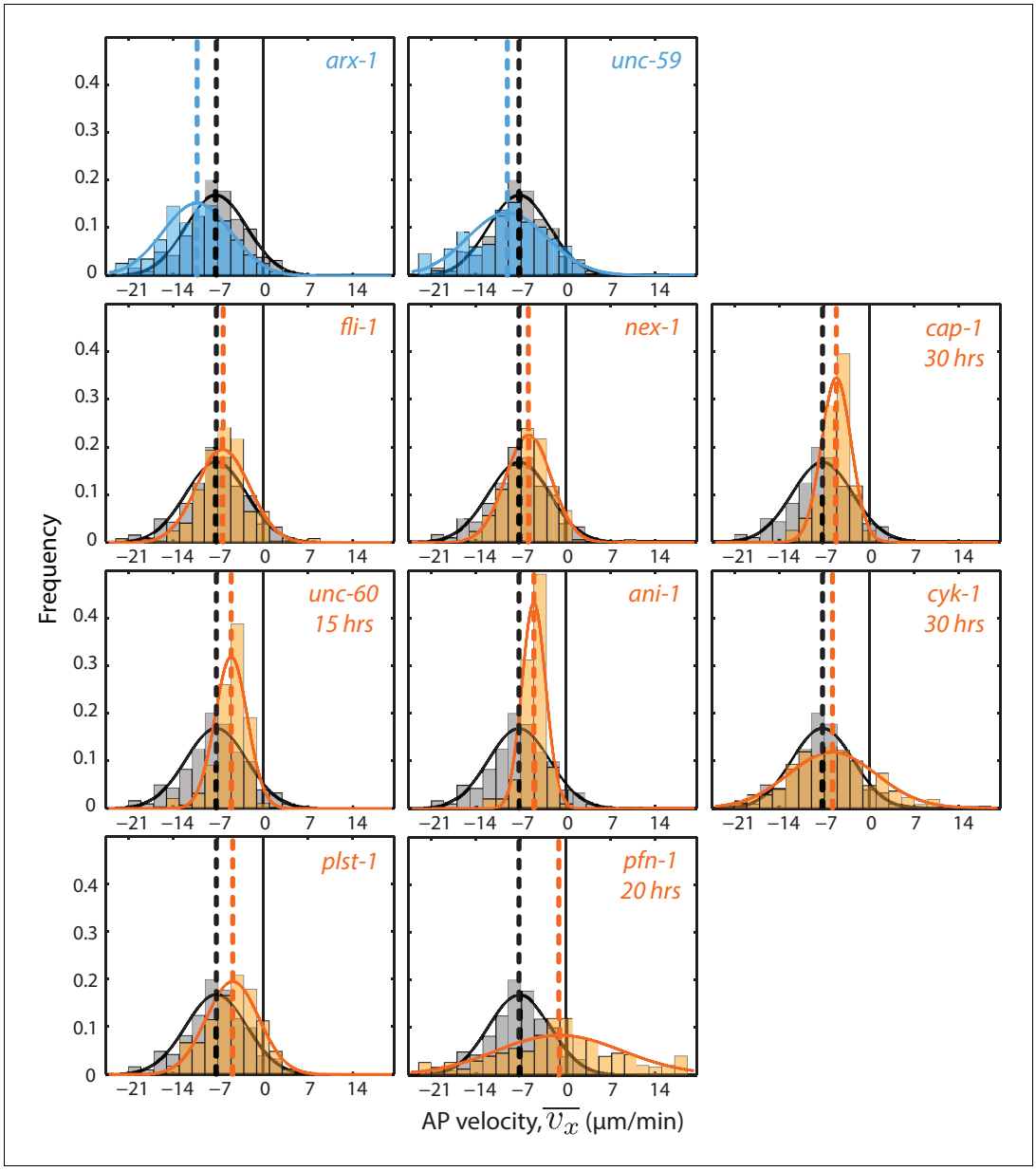

Figure 2—figure supplement 1. Comparison of mean AP velocity, $\overline{v_x}$. Each graph presents the instantaneous AP velocity $\overline{v_x}$ histogram for the RNAi condition specified. Only ABP knockdowns that are significantly different from the negative control, *klp-1 (RNAi)*, are shown. Gray histogram, *klp-1 (RNAi)* condition; dashed lines, mean $\overline{v_x}$. The number of hours of RNAi is 40 hrs, unless otherwise stated.

DOI: https://doi.org/10.7554/eLife.37677.004

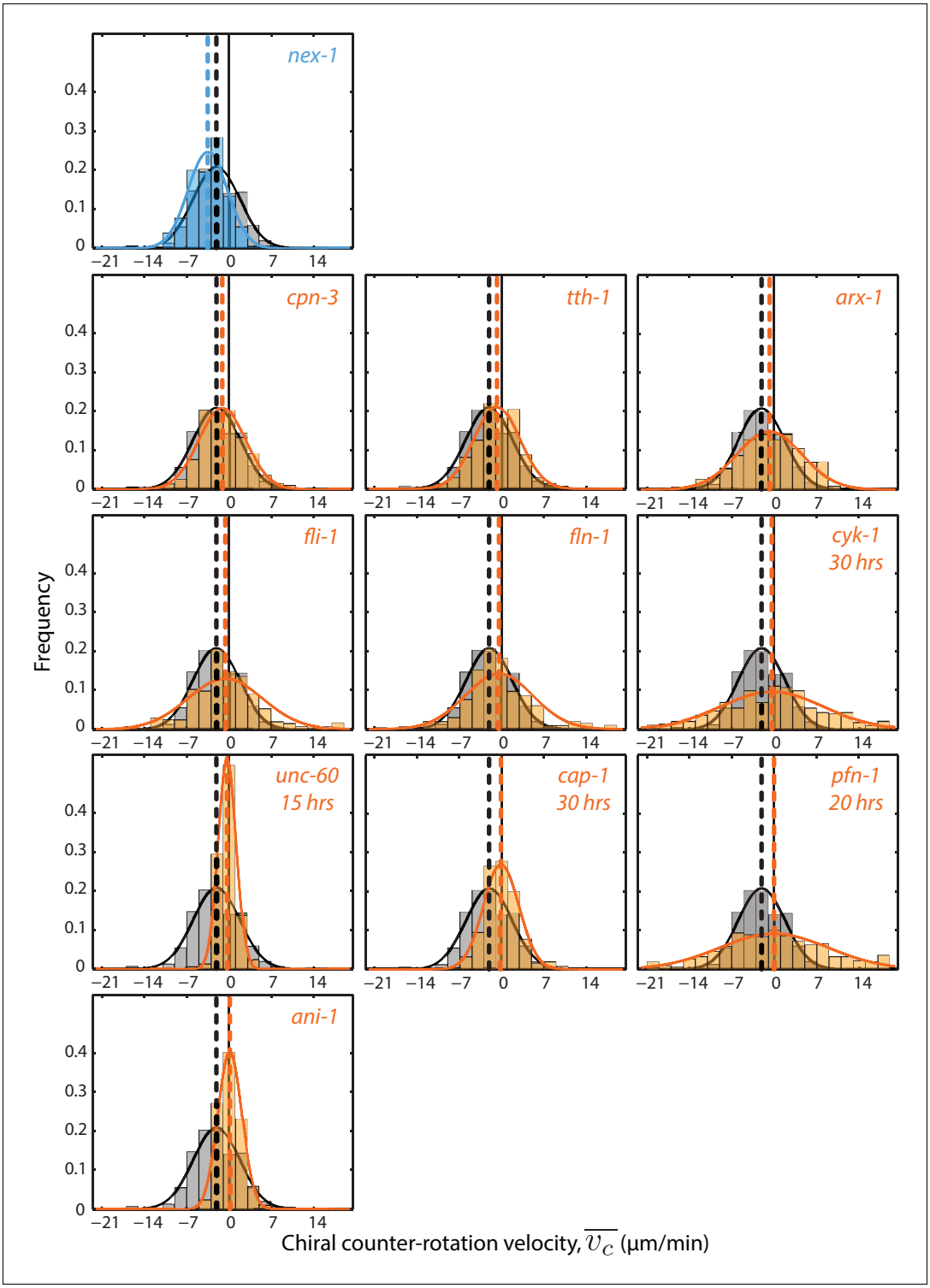

Figure 2—figure supplement 2. Comparison of mean chiral counter-rotation velocity, $\overline{v_c}$. Each graph presents the instantaneous chiral counter-rotation velocity $\overline{v_c}$ histogram for the RNAi condition specified. Only ABP knockdowns that are significantly different from the negative control, *klp-1 (RNAi)*, are shown. Gray histogram, *klp-1 (RNAi)* condition; dashed lines, mean $\overline{v_c}$. The number of hours of RNAi is 40 hrs, unless otherwise stated.

DOI: https://doi.org/10.7554/eLife.37677.005

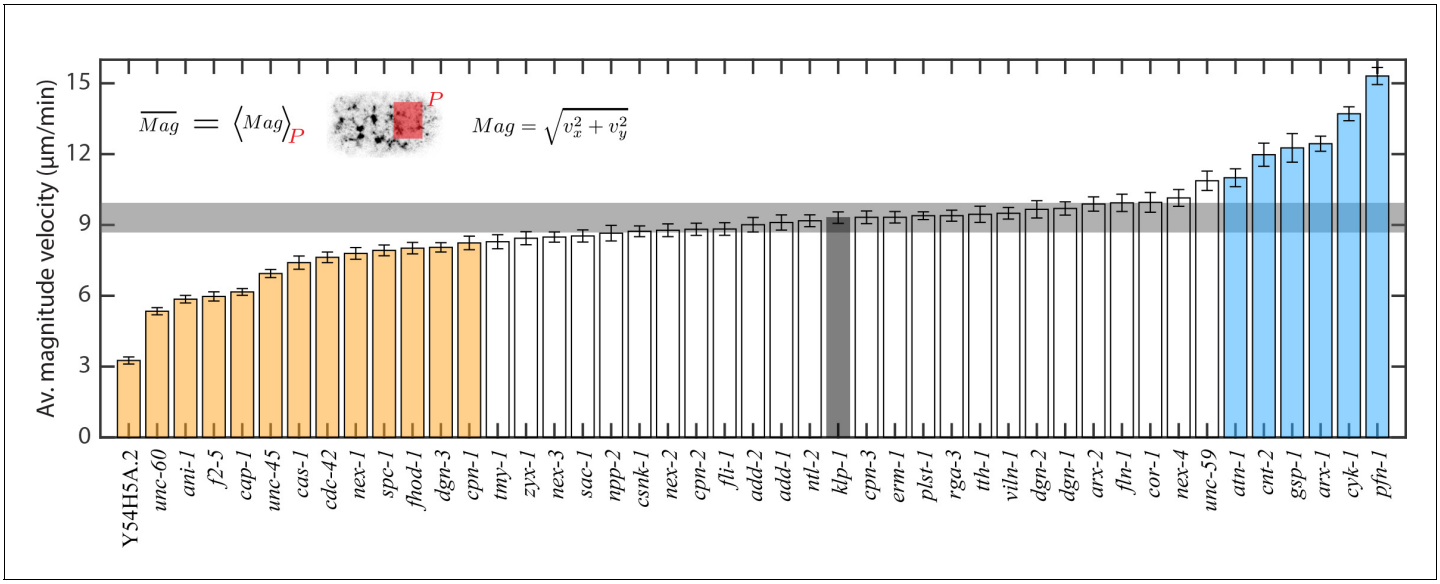

Figure 2—figure supplement 3. Comparison of mean magnitude velocity, $\overline{Mag}$. Error bars, SEM; gray bar, negative control, *klp-1 (RNAi)* condition; gray horizontal bar, error of the mean with 99% confidence for *klp-1 (RNAi)*; cyan, beige bars, significantly different knockdowns with 99% confidence (Wilcoxon rank sum test).

DOI: https://doi.org/10.7554/eLife.37677.006

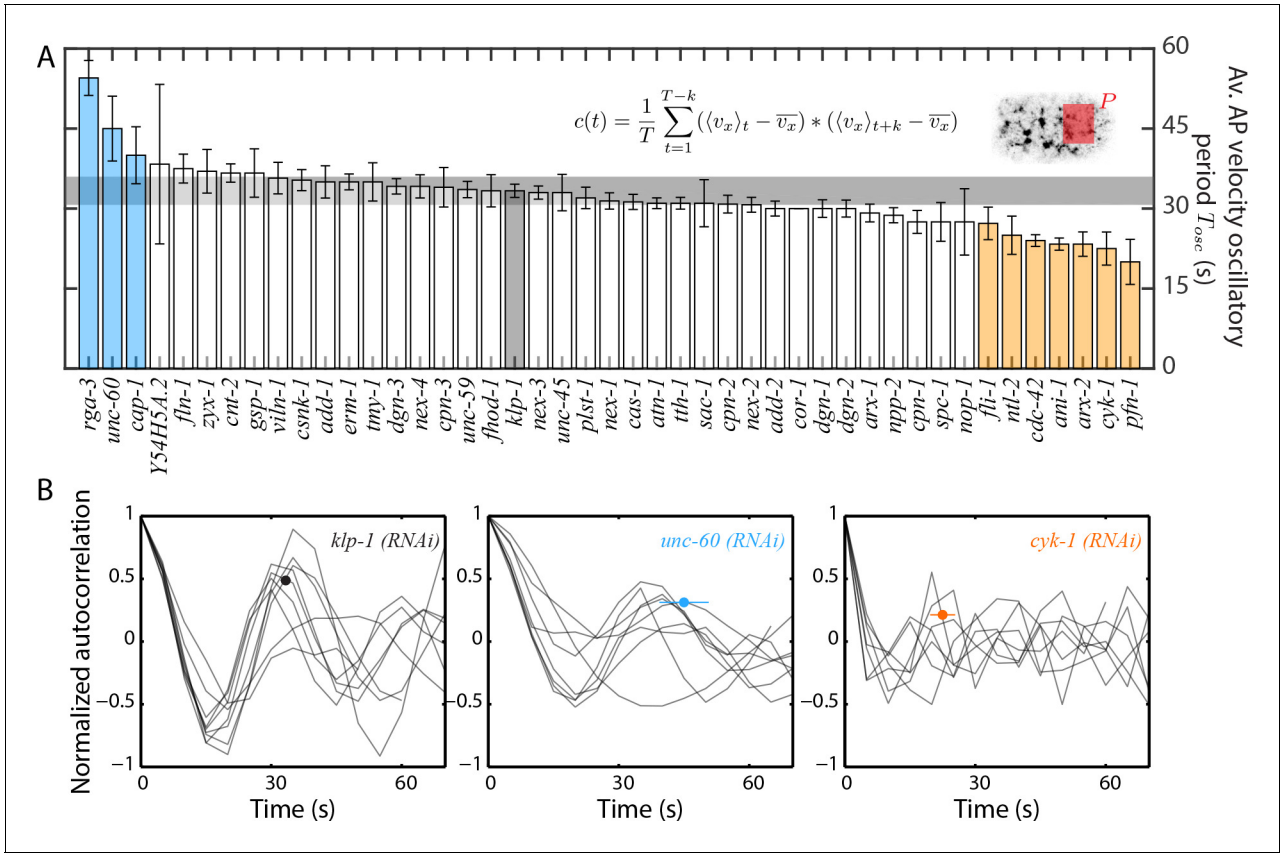

Figure 3. Quantification of pulsatile period of cortical flow. (**A**) Comparison of mean period of pulsatile AP velocity, T_{osc}, in the posterior of the embryo. Shaded area in the inset represents the region over which the spatial average of velocity was performed in each time frame. The formula for the autocorrelation function is indicated, where T is total analysis time of cortical flow and k is increment (see Materials and methods). Error bars, SEM; gray bar, negative control, *klp-1 (RNAi)* condition; gray horizontal bar, error of the mean with 95% confidence for *klp-1 (RNAi)*; cyan, beige bars, significantly different knockdowns with 95% confidence (Wilcoxon rank sum test). (**B**) Normalized autocorrelation decay curves from individual embryos (thin black lines) for the negative control, *klp-1 (RNAi)*, *cyk-1 (RNAi)* and *unc-60 (RNAi)*. Circular markers represent mean of the periods determined from individual embryos, with error bars representing SEM. See Supplementary file for number of independent embryo samples in each RNAi condition.

DOI: https://doi.org/10.7554/eLife.37677.011

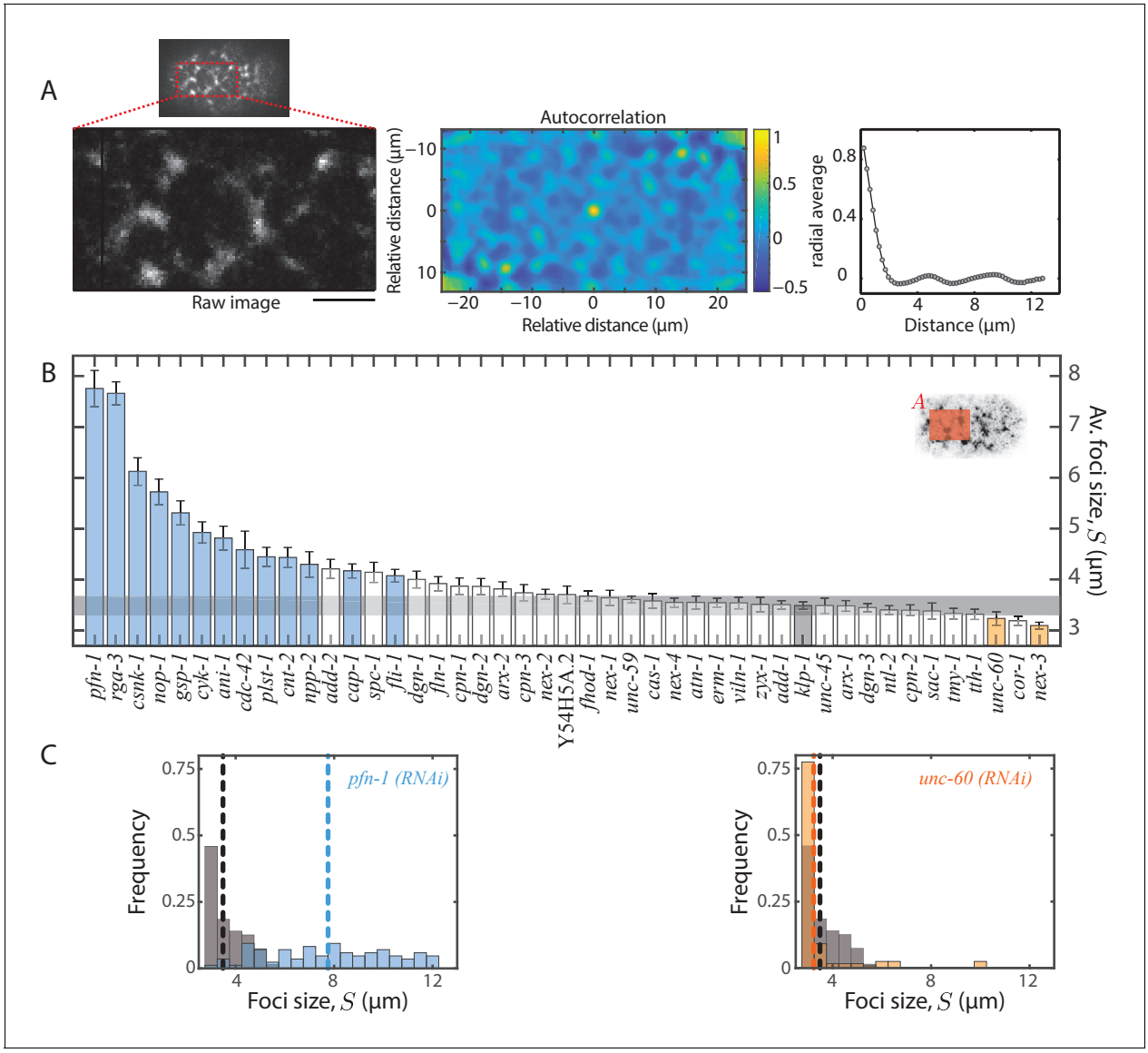

Figure 4. Quantification of myosin foci size. (**A**) Representative 2D myosin fluorescence intensity autocorrelation function as a heat map (middle) for the anterior region (left) of a single frame during cortical flow from a *klp-1 (RNAi)* embryo. Scale bar, 5 μm. Right - radial average of the autocorrelation function. (**B**) Comparison of mean foci size, *S*. Error bars, SEM; gray bar, negative control, *klp-1 (RNAi)* condition; gray horizontal bar, error of the mean with 99% confidence for *klp-1 (RNAi)*; cyan, beige bars, significantly different knockdowns with 99% confidence (Wilcoxon rank sum test). Shaded area in the inset represents the region in which the fluorescence intensity autocorrelation was performed in each frame. (**C**) Representative histograms of *S* determined over time during the cortical flow period. Gray histograms, *klp-1 (RNAi)* condition; dashed lines, mean foci size. See ***Figure 4—figure supplement 1*** for histograms of significantly different ABPs. See Supplementary file for number of independent embryo samples in each RNAi condition.

DOI: https://doi.org/10.7554/eLife.37677.013

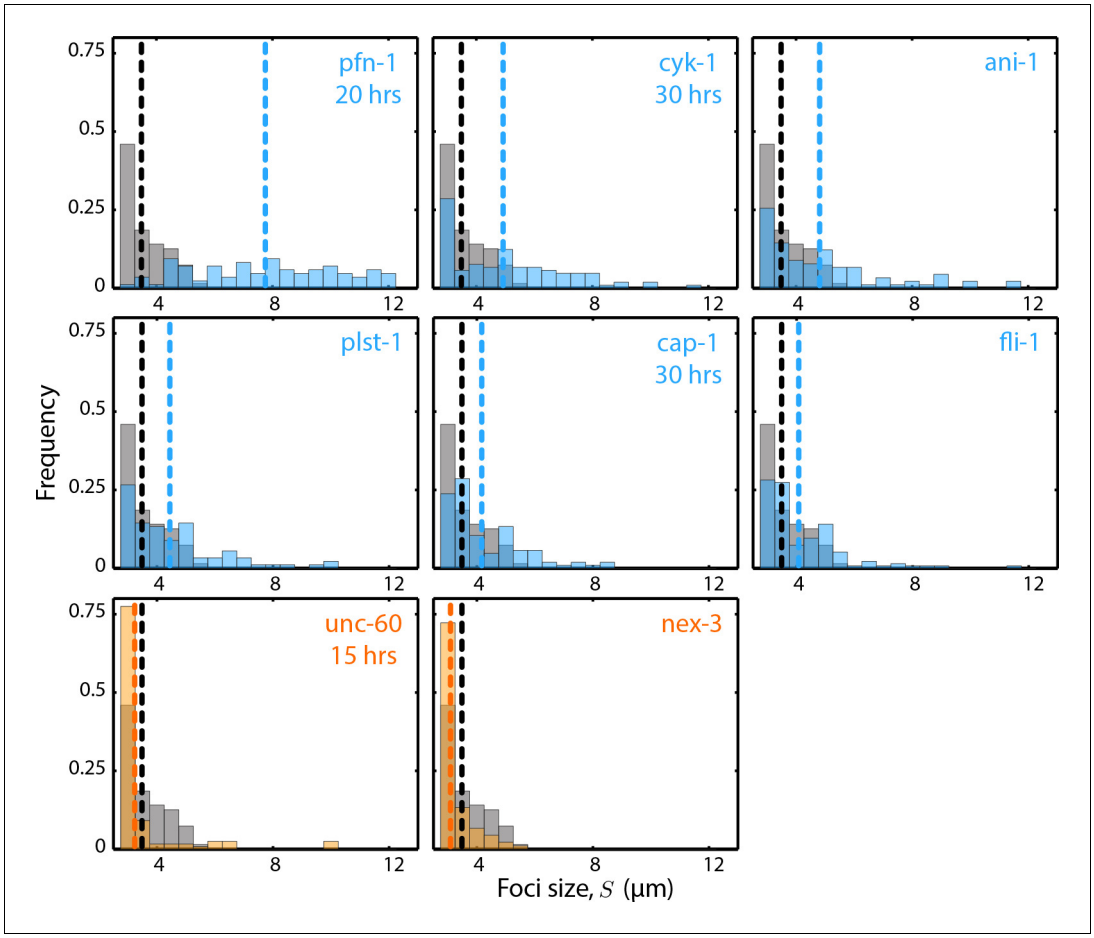

Figure 4—figure supplement 1. Comparison of mean foci size, S. Each graph presents the foci size histogram for the RNAi condition specified. Only ABP knockdowns that are significantly different from the negative control, *klp-1 (RNAi)*, are shown. Gray histogram, *klp-1 (RNAi)* condition; dashed lines, mean S. The number of hours of RNAi is 40 hrs, unless otherwise stated.

DOI: https://doi.org/10.7554/eLife.37677.014

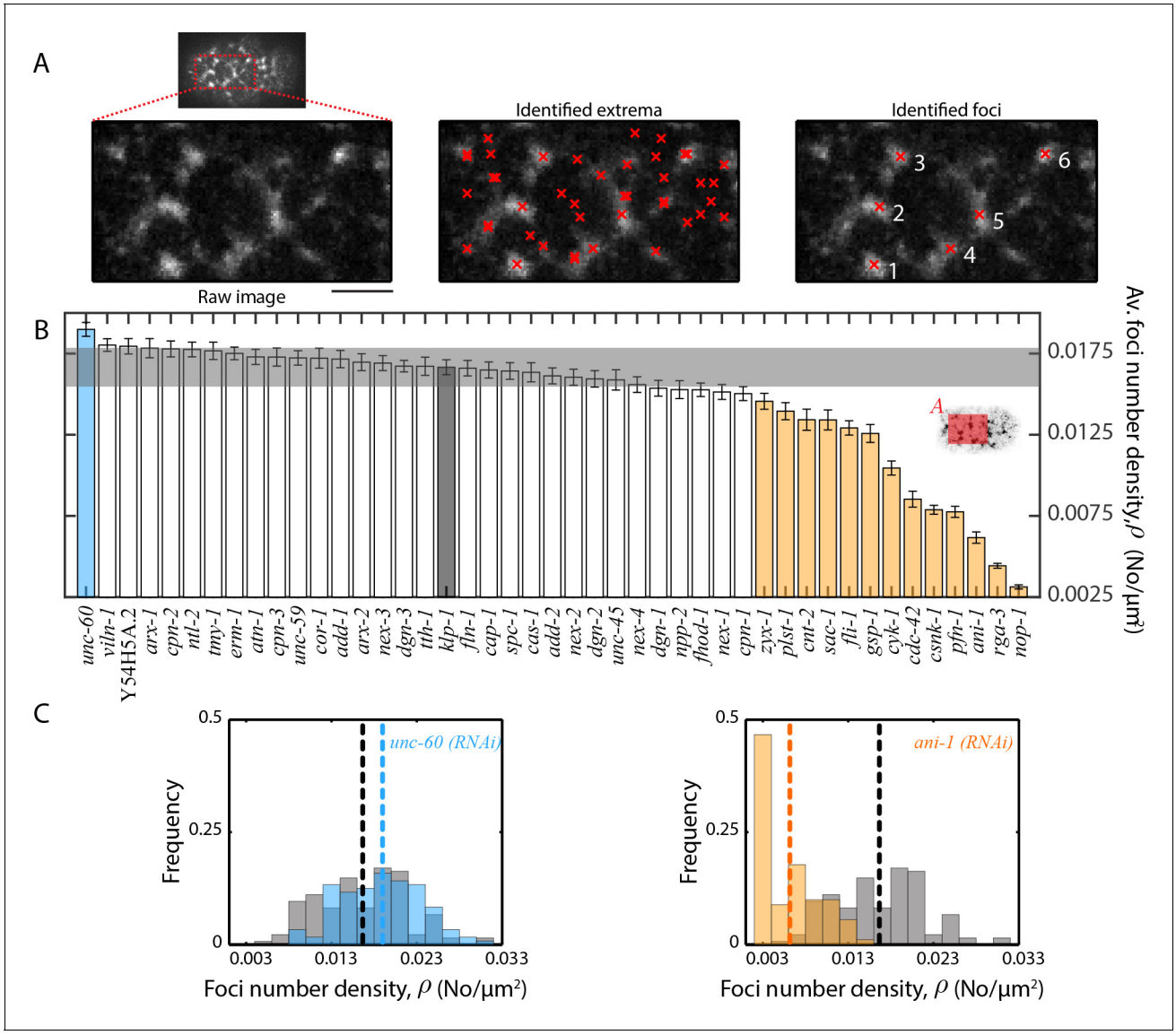

Figure 5. Quantification of myosin foci number density. (**A**) Detection of myosin foci (right) by analysis of local changes in fluorescence intensity in the vicinity of identified local extrema (middle) for the anterior region (left) of a single frame during cortical flow from a *klp-1 (RNAi)* embryo. Scale bar, 5 μm. (**B**) Comparison of mean foci number density, ρ. Error bars, SEM; gray bar, negative control, *klp-1 (RNAi)* condition; gray horizontal bar, error of the mean with 99% confidence for *klp-1 (RNAi)*; cyan, beige bars, significantly different knockdowns with 99% confidence (Wilcoxon rank sum test). Shaded area in the inset represents the region that was utilized for foci detection in each frame. (**C**) Representative histograms of ρ determined over time during the cortical flow period. Gray histograms, *klp-1 (RNAi)* condition; dashed lines, mean foci number density. See ***Figure 5—figure supplement 1*** for histograms of significantly different ABPs. See Supplementary file for number of independent embryo samples in each RNAi condition.

DOI: https://doi.org/10.7554/eLife.37677.015

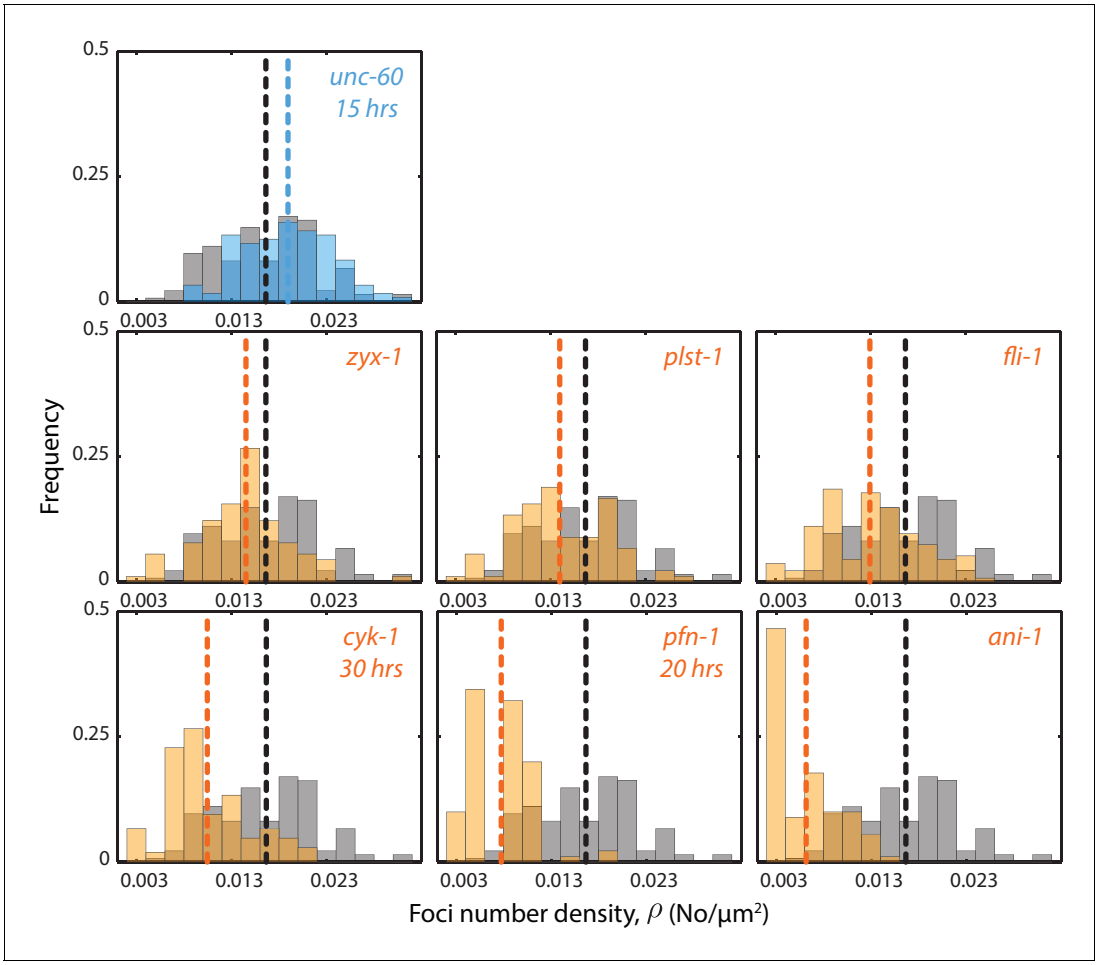

Figure 5—figure supplement 1. Comparison of mean foci number density, ρ. Each graph presents the foci number density histogram for the RNAi condition specified. Only ABP knockdowns that are significantly different from the negative control, *klp-1 (RNAi)*, are shown. Gray histogram, *klp-1 (RNAi)* condition; dashed lines, mean ρ. The number of hours of RNAi is 40 hrs, unless otherwise stated.

DOI: https://doi.org/10.7554/eLife.37677.016

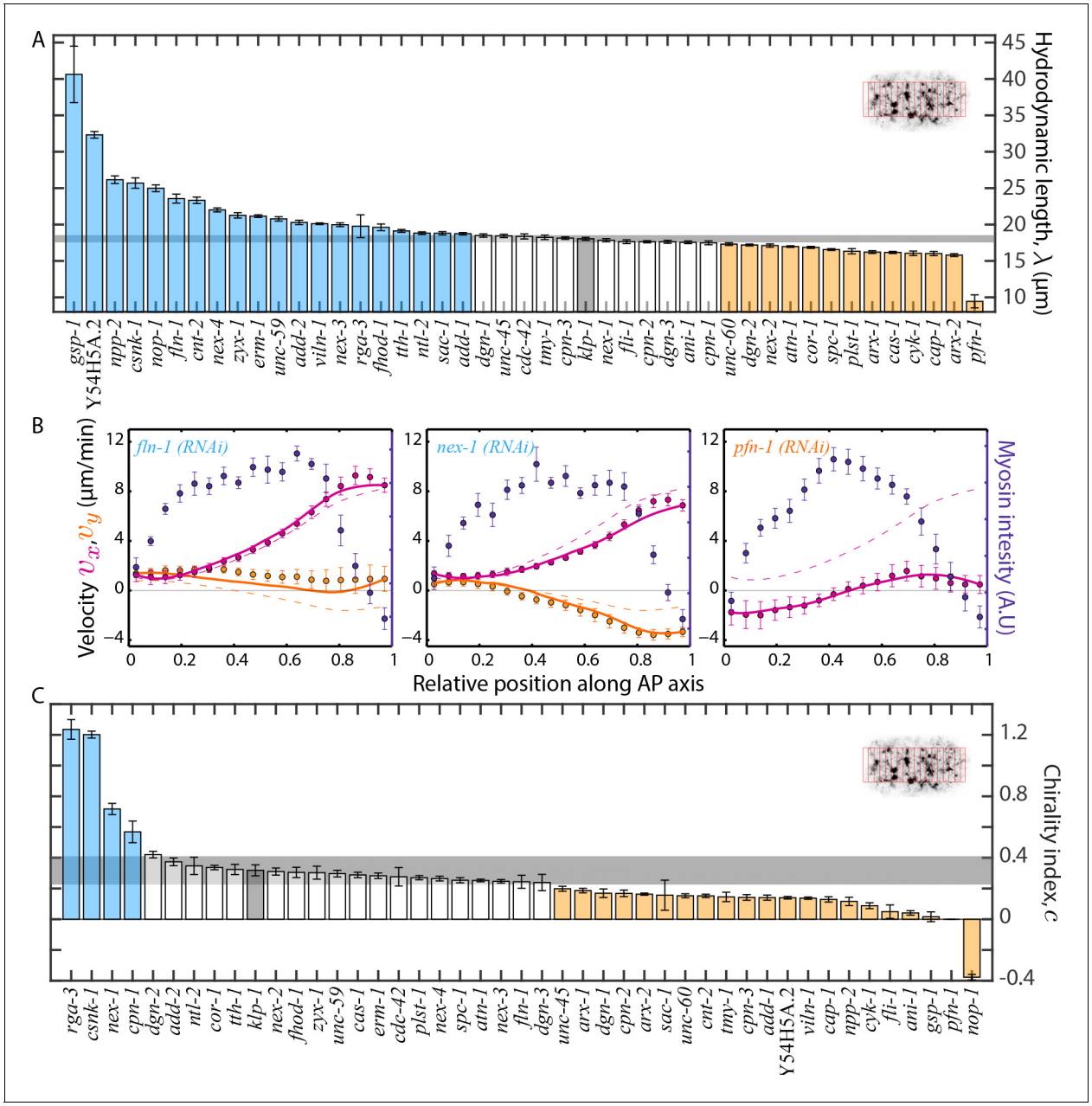

Figure 6. Estimation of physical properties of the cortex. (**A**), (**C**) Comparison of the hydrodynamic length, λ and chirality index, c of the cortex respectively. Error bars, SEM; gray bar, negative control, *klp-1 (RNAi)* condition; gray horizontal bar, error of the mean with 99% confidence for *klp-1 (RNAi)*; cyan, beige bars, significantly different knockdowns with 99% confidence (significance determined using normal cumulative distribution function in MATLAB). The bins over which spatial average of velocities were determined in each frame are shown in the inset. (**B**) Average myosin intensity (blue markers) and velocity profiles (magenta markers, AP flow velocity v_x; beige markers, y-velocity v_y) along the AP axis for representative RNAi conditions. Error bars, SEM. Magenta and beige curves, respective theoretical velocity profiles. Dashed lines, theoretical velocity profiles for *klp-1 (RNAi)* condition. See ***Figure 6—figure supplement 1*** for more examples of fit profiles of significantly different ABPs. See Supplementary file for number of independent embryo samples in each RNAi condition.

DOI: https://doi.org/10.7554/eLife.37677.017

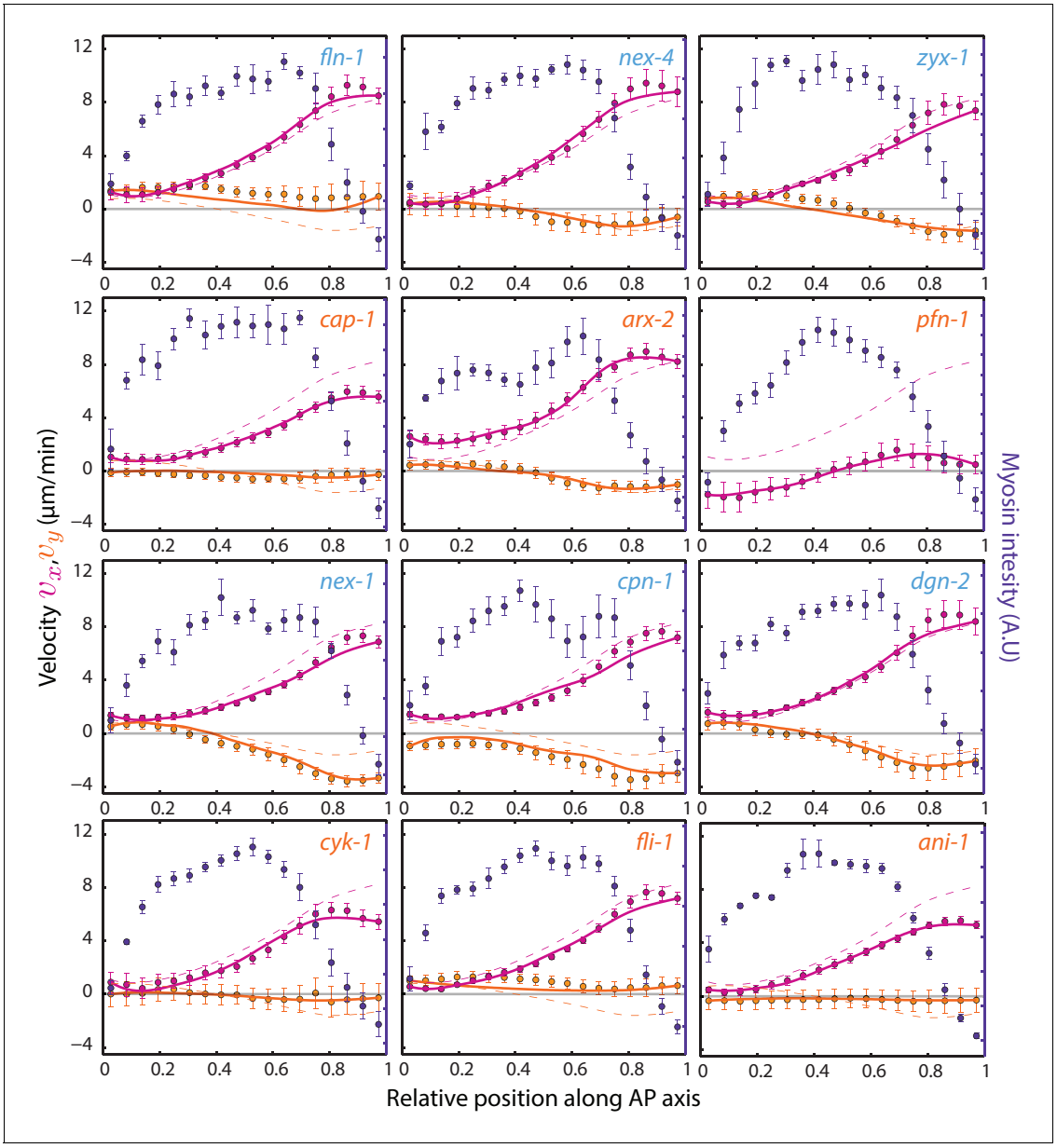

Figure 6—figure supplement 1. Comparison of hydrodynamic model fit to experimental flow profiles. Row 1 (row 2) represents the top three ABP knockdowns that resulted in a significantly higher (lower) λ, and row 3 (row 4) represents the top three ABP knockdowns that resulted in a significantly higher (lower) c. Each graph presents the average myosin intensity (blue markers) and velocity profiles (magenta markers, AP flow velocity v_x; beige markers, y-velocity v_y) along the AP axis for each RNAi condition specified. Error bars, SEM. Magenta and beige curves, respective theoretical velocity profiles. Dashed lines, theoretical velocity profiles of the negative control, *klp-1 (RNAi)*.

DOI: https://doi.org/10.7554/eLife.37677.018

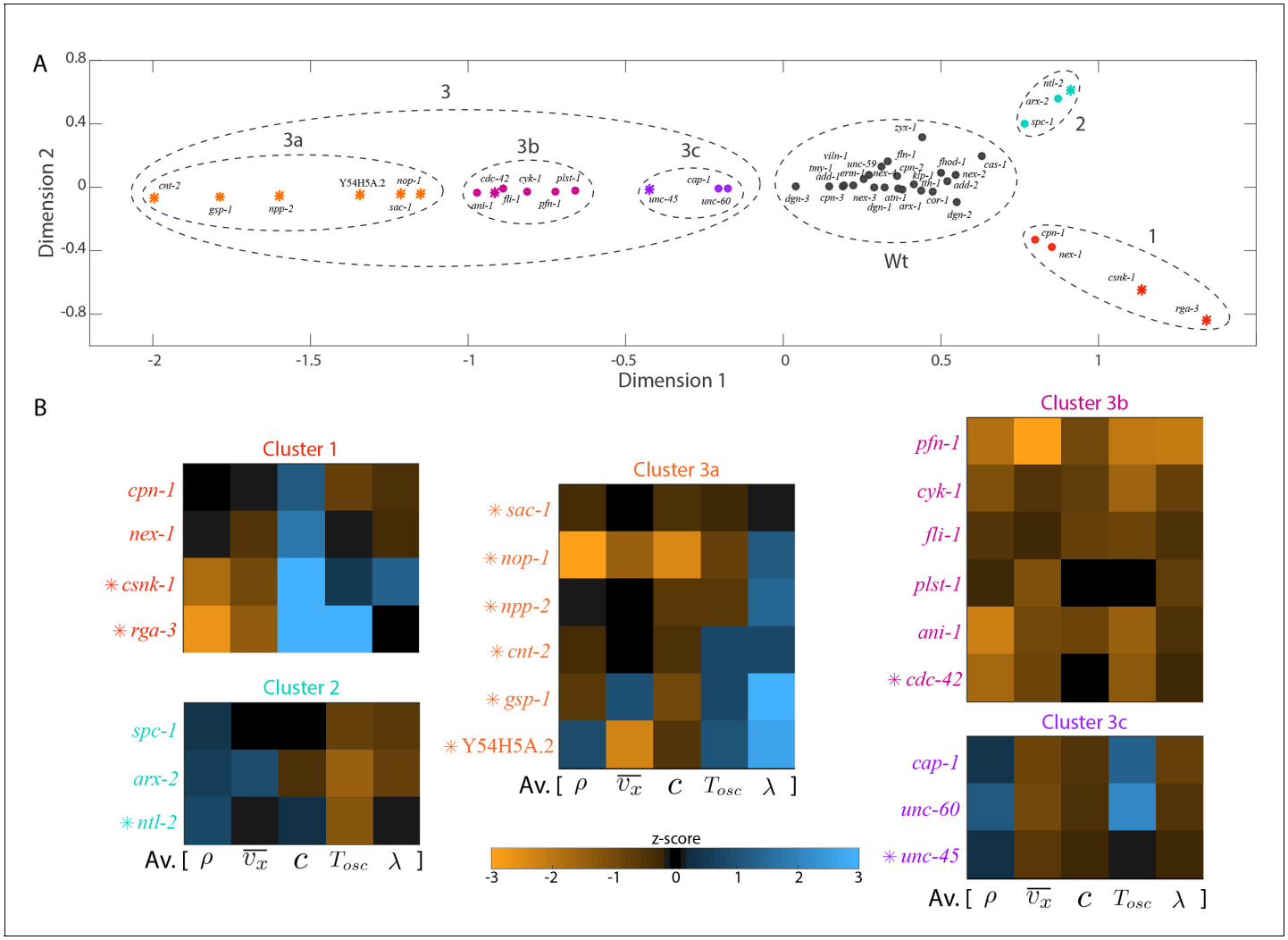

Figure 7. Distinct molecular functions possess similar roles at large-scales. (**A**) Non-linear dimensional reduction of the quantitative data set was performed and plotted along dimensions that represent the highest variability. Circular markers, ABPs; star markers, actomyosin regulators; colours represent the different clusters and black represents knockdowns in the same group as the negative control, *klp-1 (RNAi)*; Wt - wild type. See ***Figure 7—figure supplement 1*** for a heat map of the wild type cluster and ***Figure 7—figure supplement 4*** for a correlation of quantifications and the two principal axes of the dimensionally reduced data set. (**B**) Parameters that were used for dimensional reduction (foci density ρ, AP velocity $\overline{v_x}$, chirality index c, flow period T_{osc}, hydrodynamic length λ) were rearranged and displayed as heat maps for knockdowns that constitute each cluster. Colour bar, z-score. See ***Figure 7—figure supplement 2*** for correlations between different quantifications and ***Figure 7—figure supplement 3*** for visualisation of cytoplasmic actin fluorescence for *unc-60* and *cap-1 (RNAi)* from cluster 3c.

DOI: https://doi.org/10.7554/eLife.37677.019

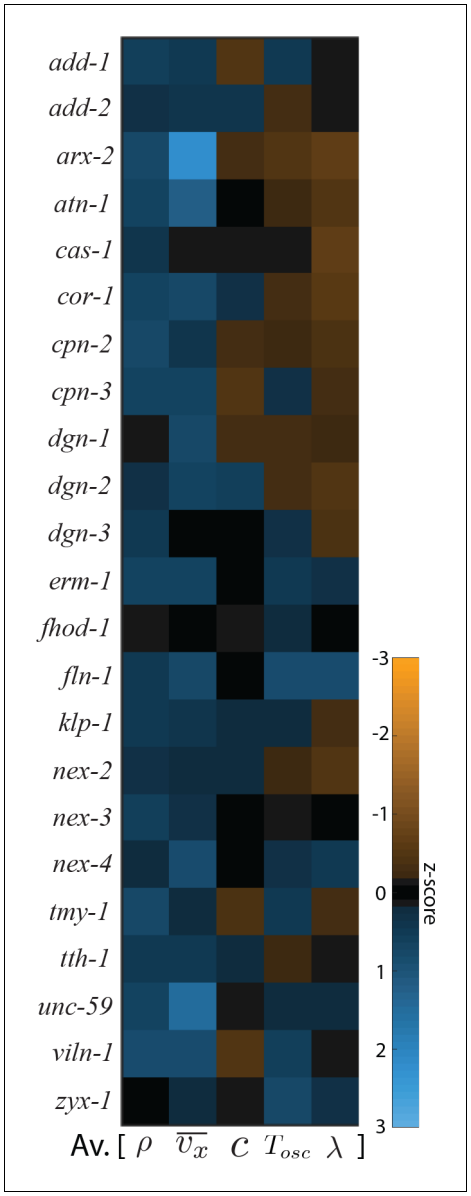

Figure 7—figure supplement 1. Heat map of proteins part of the wild type cluster. Parameters that were used for dimensional reduction (foci density ρ, AP velocity $\overline{v_x}$, chirality index c, flow period T_{osc}, hydrodynamic length λ) are displayed as heat maps for knockdowns that constitute the wild type cluster. Colour bar, z-score; *klp-1 (RNAi)* - negative control.
DOI: https://doi.org/10.7554/eLife.37677.020

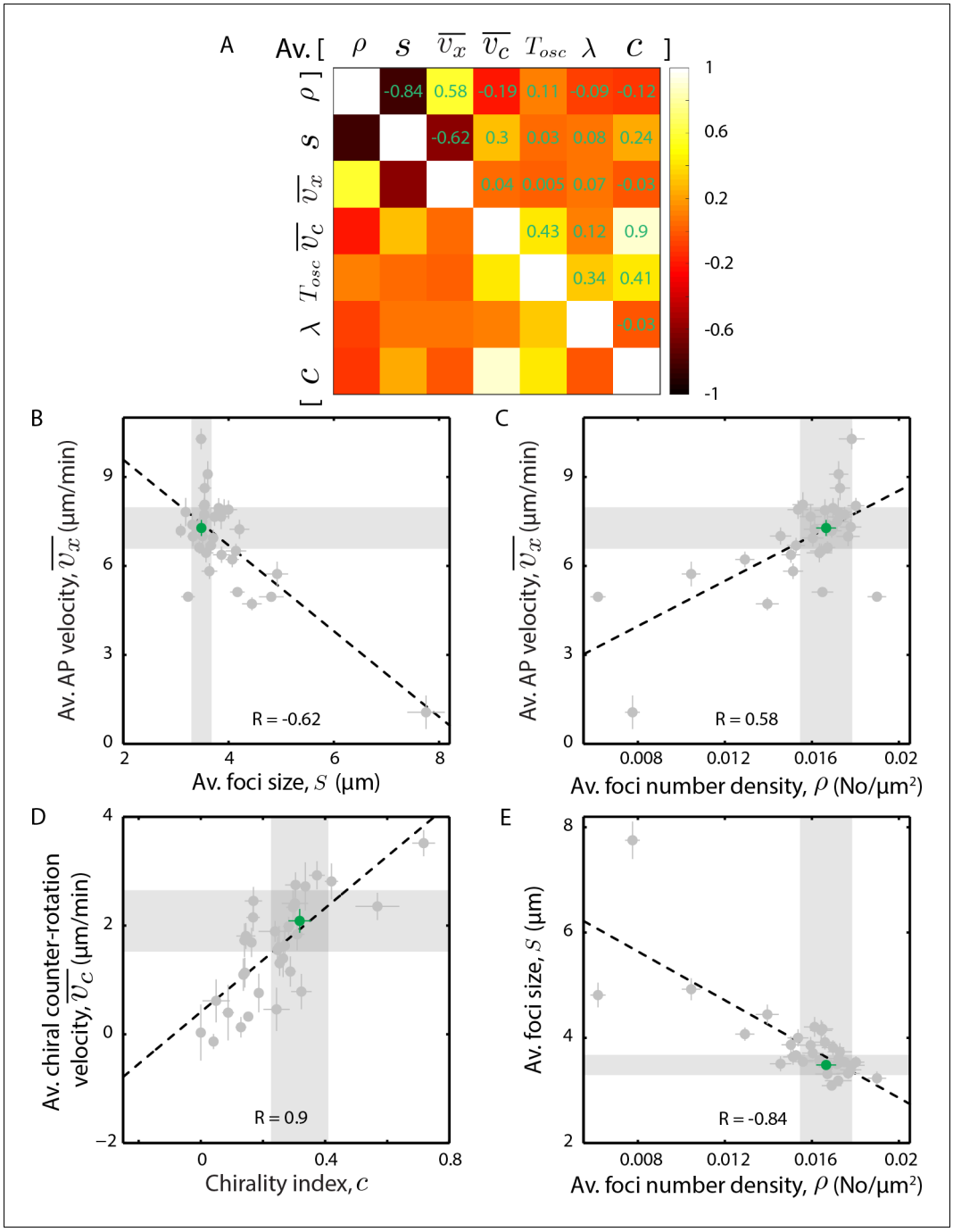

Figure 7—figure supplement 2. Correlation between quantifications for ABPs. (**A**) Pearson's linear correlation coefficients between pairs of quantifications are shown as a heat map. (**B**)-(**E**) Selected pairs of quantifications that were positively or negatively correlated are shown as scatter plots. Circular markers, individual knockdowns; error bars, SEM; green marker, negative control, *klp-1 (RNAi)*; gray bars, error of the mean with 99% confidence for *klp-1 (RNAi)* condition; dashed line, least squares fit of the data.

DOI: https://doi.org/10.7554/eLife.37677.021

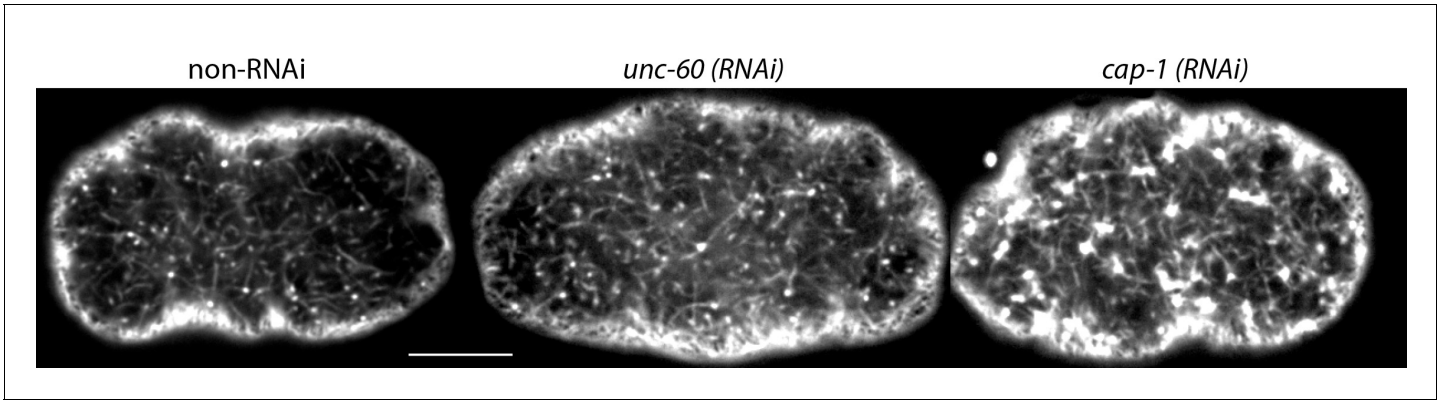

Figure 7—figure supplement 3. Cytoplasmic actin fluorescence. SWG007 transgenic line was used to image cytoplasmic actin. A snapshot of the indicated knockdown was performed 2 μm deeper from the cortical region at the start of cortical flows and displayed. An increase in cytoplasmic actin fluorescence was observed in *unc-60* and *cap-1 (RNAi)* conditions compared to the negative control, *klp-1 (RNAi)*. Images are displayed in the same gray-scale dynamic range. Scale bar, 10 μm.

DOI: https://doi.org/10.7554/eLife.37677.022

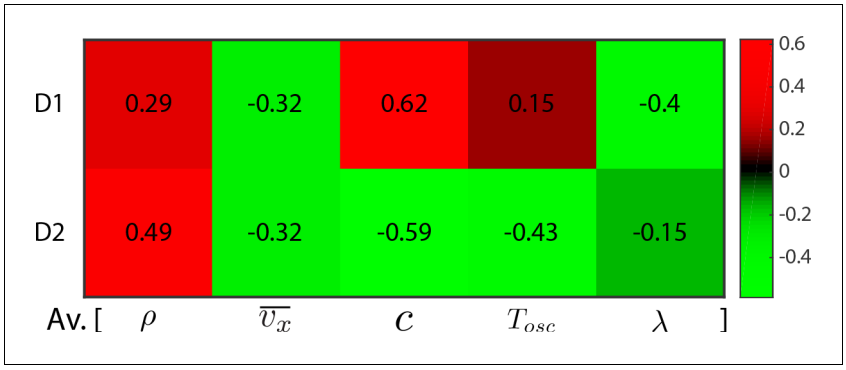

Figure 7—figure supplement 4. Correlation between quantifications and clustering dimensions. Correlation between the five quantifications (foci density ρ, AP velocity $\overline{v_x}$, chirality index c, flow period T_{osc}, hydrodynamic length λ) used for clustering and the two principal axes (D1, D2) in the dimensionally reduced data set are shown as a heat map. The Pearson's linear correlation co-efficient is indicated in each heat map square.

DOI: https://doi.org/10.7554/eLife.37677.023